

Cosmic Microwave Background Map-Making Solutions Often Improve With Cooling

BAI-QIANG QIANG¹ AND KEVIN M. HUFFENBERGER¹ 

¹*Department of Physics, Florida State University, Tallahassee, Florida 32306*

ABSTRACT

In the context of Cosmic Microwave Background data analysis, we study the solution to the equation that transforms scanning data into a map. As originally suggested in “messenger” methods for solving linear systems, we split the noise covariance into uniform and non-uniform parts and adjust their relative weight during the iterative solution. With simulations we study systems that have different noise properties, and find that this “cooling” or perturbative approach is particularly effective when there is significant low-frequency noise in the timestream. In such cases, a conjugate gradient algorithm applied to this modified system converges faster and to a higher fidelity solution than the standard conjugate gradient approach. We give an analytical expression for the parameter that controls how gradually the linear system changes during the course of the solution.

Keywords: Computational methods — Cosmic microwave background radiation — Astronomy data reduction

1. INTRODUCTION

In observations of the Cosmic Microwave Background (CMB), map-making is an intermediate step between the collection of raw scanning data and the scientific analyses, such as the estimation of power spectra and cosmological parameters. Next generation CMB observations will generate much more data than those today, and so it is worth exploring efficient ways to process the data, even though, on paper, the map-making problem has long been solved.

The time-ordered scanning data is summarized by

$$\mathbf{d} = P\mathbf{m} + \mathbf{n} \quad (1)$$

where \mathbf{d} , \mathbf{m} , and \mathbf{n} are the vectors of time-ordered data (TOD), the CMB sky-map signal, and measurement noise. P is the sparse matrix that encodes the telescope’s pointing. Of several map-making methods (Tegmark 1997), one of the most common is the method introduced for the Cosmic Background Explorer (COBE, Janssen & Gulkis 1992). This optimal, linear solution is

$$(P^\dagger N^{-1} P)\hat{\mathbf{m}} = P^\dagger N^{-1} \mathbf{d} \quad (2)$$

where $\hat{\mathbf{m}}$ provides the generalized least squares minimization of the χ^2 statistic,

$$\chi^2(\mathbf{m}) \equiv (\mathbf{d} - P\mathbf{m})^\dagger N^{-1} (\mathbf{d} - P\mathbf{m}). \quad (3)$$

Here we assume that the noise has zero mean $\langle \mathbf{n} \rangle = \mathbf{0}$, and noise covariance matrix $N = \langle \mathbf{nn}^\dagger \rangle$ is diagonal in frequency space. Thus map-making is a standard linear regression problem. In the case where the noise is Gaussian, the COBE solution is also the maximum likelihood solution.

With current computational power, we cannot solve for $\hat{\mathbf{m}}$ by calculating $(P^\dagger N^{-1} P)^{-1} P^\dagger N^{-1} \mathbf{d}$ directly. The noise covariance matrix N is often sparse in frequency domain and the pointing matrix P is sparse in the time-by-pixel domain. In experiments currently under design, there may be $\sim 10^{16}$ time samples and $\sim 10^9$ pixels, so these matrix inversions are intractable unless the covariance is uniform. We can use iterative methods, such as conjugate gradient descent, to avoid the matrix inversions, and execute each matrix multiplication in a basis where the matrix is sparse, using a fast Fourier transform to go between the frequency and time domain.

As an alternative to conjugate gradient descent, Huf-
fenger & Naess (2018) showed that the “messenger” iterative method could be adapted to solve the linear map-making system, based on the approach from Elsner & Wandelt (2013) to solve the linear Wiener filter. This technique splits the noise covariance into a uniform part and the remainder, and introduces an additional vector that represent the signal plus uniform noise. This messenger field acts as an intermediary between the signal and the data and has a covariance that

is conveniently sparse in every basis. [Elsner & Wandelt \(2013\)](#) also introduced a cooling scheme that takes advantage of the split covariance: over the course of the iterative solution, we adjust the relative weight of the two parts. Starting with the uniform covariance, the modified linear system gradually transforms to the final system, under the control of a cooling parameter. In numerical experiments, [Huffenberger & Naess \(2018\)](#) found that a map produced by the cooled messenger method converged significantly faster than for standard conjugate gradient methods, and to higher fidelity, especially on large scales.

[Papež et al. \(2018\)](#) showed that the messenger field approach is equivalent to a fixed point iteration scheme, and studied its convergence properties in detail. Furthermore, they showed that the split covariance and the modified system that incorporates the cooling can be solved by other means, including a conjugate gradient technique, which should generally show better convergence properties than the fixed-point scheme. However in numerical tests, [Papež et al. \(2018\)](#) did not find benefits to the cooling modification of the map-making system, in contrast to the findings of [Huffenberger & Naess \(2018\)](#).

In this paper, we show that the difference arose because the numerical tests in [Papež et al. \(2018\)](#) used much less low-frequency (or $1/f$) noise than [Huffenberger & Naess \(2018\)](#), and show that the cooling technique improves map-making performance especially when the low-frequency noise is large. This performance boost depends on a proper choice for the pace of cooling. [Kodi Ramanah et al. \(2017\)](#) showed that for Wiener filter the cooling parameter should be chosen as a geometric series. In this work, we give an alternative interpretation of the parameterizing process and show that for map-making the optimal choice (unsurprisingly) is also a geometric series.

In Section 2 we describe our methods for treating the map-making equation and our numerical experiments. In Section 3 we present our results. In Section 4, we list our conclusions. In Appendix A we derive the prescription for our cooling schedule.

METHODS

2.1. Parameterized Conjugate Gradient Method

The messenger field approach introduced an extra cooling parameter λ to the map-making equation, and solved the linear system with the alternative parameterized covariance $N(\lambda) = \lambda\tau I + \bar{N}$. The parameter $\tau = \min(\text{diag}(N))$ represents the uniform level of (white) noise in the original covariance. $\bar{N} \equiv N - \tau I$ is the non-uniform part of the original noise covariance.

(Here N without any arguments denotes the original noise covariance matrix $N = \langle \mathbf{nn}^\dagger \rangle$.) In this work we find it more convenient to work with the reciprocal of the cooling parameter $\eta = \lambda^{-1}$ which represents the degree of heteroscedasticity (non-uniformity) in the parameterized covariance

$$N(\eta) = \tau I + \eta \bar{N}, \quad (4)$$

a choice that leads to the same system of map-making equations. (This is because $N(\eta) = \lambda^{-1}N(\lambda)$ and the map-making equation (5) is insensitive to scalar multiples of the covariance.) When $\eta = 1$ this parameterized covariance $N(\eta)$ equals N .

[Papež et al. \(2018\)](#) showed that the conjugate gradient method can be easily applied to the cooled map-making problem. In our notation, this is equivalent to iterating on the parameterized map-making equation

$$(P^\dagger N(\eta_i)^{-1} P) \hat{\mathbf{m}}(\eta_i) = P^\dagger N(\eta_i)^{-1} \mathbf{d}, \quad (5)$$

as we adjust the parameter through a set of levels $\{\eta_i\}$. (We use $\hat{\mathbf{m}}$ with no η argument to mean the estimated $\hat{\mathbf{m}}$ in Eq. (2), independent of η .) We could define $A(\eta) \equiv P^\dagger N(\eta)^{-1} P$ and $b(\eta) \equiv P^\dagger N(\eta)^{-1} \mathbf{d}$, and equation (5) could be written as $A(\eta_i) \hat{\mathbf{m}}(\eta_i) = b(\eta_i)$.

In our numerical experiments, we confirm that the conjugate gradient approach is converging faster than the fixed point iterations suggested by the messenger map-making method in [Huffenberger & Naess \(2018\)](#). For concreteness we fix the preconditioner to $M = P^\dagger P$ for all calculations.

When $\eta = 0$, the noise covariance matrix $N(0)$ is homoscedastic (uniform), and solution is given by simple binned map $\hat{\mathbf{m}}(0) = (P^\dagger P)^{-1} P^\dagger \mathbf{d}$, which can be solved directly.

Since the non-white part \bar{N} is the troublesome portion of the covariance, we can think of the η parameter as increasing the heteroscedasticity of the system, adding a perturbation to the solution achieved at a particular stage, building ultimately upon the initial uniform covariance model. Therefore, this quasi-static process requires η increase as $0 = \eta_0 \leq \eta_1 \leq \dots \leq \eta_{\text{final}} = 1$, at which point we arrive at the desired map-making equation, and the solution $\hat{\mathbf{m}}(1) = \hat{\mathbf{m}}$.

We may iterate more than once at each intermediate η_i : we solve with conjugate gradient iterations using the result from previous calculation $\hat{\mathbf{m}}(\eta_{i-1})$ as the initial value, and move to next parameter η_{i+1} when the norm of residual vector

$$\|\mathbf{r}(\mathbf{m}, \eta_i)\| \equiv \|P^\dagger N(\eta_i)^{-1} P \mathbf{m} - P^\dagger N(\eta_i)^{-1} \mathbf{d}\| \quad (6)$$

is an order of magnitude smaller than the norm of the right hand side of Eq. (5).

$$\|\mathbf{r}(\mathbf{m}, \eta_i)\| < 0.1 \|P^\dagger N(\eta_i)^{-1} \mathbf{d}\| \quad (7)$$

This is not stringent enough to completely converge at this η -level, but we find that it causes the system to converge sufficiently to allow us to move on to the next η .

2.2. Analytical expression for $\{\eta_i\}$ series

The next question is how to appropriately choose these monotonically increasing parameters η . We also want to determine $\eta_1, \dots, \eta_{n-1}$ before starting conjugate gradient iterations, because the time ordered data \mathbf{d} is very large, and we do not want to keep it in the system memory during calculation. If we determine $\eta_1, \dots, \eta_{n-1}$ before the iterations, then we can precompute the right-hand side of Eq. (5) for each η_i and keep these map-sized objects in memory, instead of the entire time-ordered data.

In Appendix A, we show that a generic good choice for the η parameters are the geometric series

$$\eta_i = \min \left\{ (2^i - 1) \frac{\tau}{\max(\bar{N}_f)}, 1 \right\}, \quad (8)$$

where \bar{N}_f are the eigenvalues of \bar{N} under frequency representation. This is one of our main results. It tells us not only how to choose parameters η_i , but also when we should stop the perturbation, and set $\eta = 1$. For example, if noise covariance matrix N is almost white noise, then $\bar{N} = N - \tau I \approx 0$, and we would have $\tau / \max(\bar{N}_f) > 1$. This tell us that we don't need to use parameterized method at all, because $\eta_0 = 0$ and $\eta_1 = \eta_2 = \dots = 1$. This corresponds to the standard conjugate gradient method with simple binned map as the initial guess (as recommended by Papež et al. 2018).

2.3. Intuitive Interpretation of η

Here is a way to interpret the role of η that is less technical than Appendix A. Our ultimate goal is to find $\hat{\mathbf{m}}(1)$ which minimizes $\chi^2(\mathbf{m})$ in Eq. (3). Since N is diagonal in frequency space, χ^2 could be written as a sum of all frequency mode $|(\mathbf{d} - P\mathbf{m})_f|^2$ with weight N_f^{-1} , such as $\chi^2(\mathbf{m}) = \sum_f |(\mathbf{d} - P\mathbf{m})_f|^2 N_f^{-1}$. The weight is large for low-noise frequency modes (small N_f), and small for high-noise modes. Which means $\chi^2(\mathbf{m})$ would favor the low-noise modes, and therefore conjugate gradient map-making $\hat{\mathbf{m}}$ focuses on minimizing the error $\boldsymbol{\varepsilon} \equiv \mathbf{d} - P\mathbf{m}$ in the low-noise part.

After introducing η , we minimize $\chi^2(\mathbf{m}, \eta)$ in Eq. (A1) instead. For $\eta = 0$, $N^{-1}(0) \propto I$ the system is homoscedastic and the estimated map $\hat{\mathbf{m}}(0)$ does not prioritize any frequency mode. As we slowly increase η , we

decrease the weight for the high noise modes, and focusing minimizing error for low noise part. If we start with $\eta_1 = 1$ directly, which corresponds to the vanilla conjugate gradient method, then the conjugate gradient solver will focus most on minimizing the low noise part, such that χ^2 would converge very fast on low-noise modes, but slowly on the high-noise part. It may get stuck at some local minimum point in χ^2 and have trouble getting to the global minimum. However by introducing η parameter, we let the solver first treat every frequency equally, then as η slowly increases, it gradually give more focus to the lowest noise part.

2.4. Computational Cost

To properly compare the performance cost of this method with respect to vanilla conjugate gradient method with simple preconditioner, we need to compare their computational cost at each iteration. The right hand side of parameterized map-making equation (5) $b(\eta_i)$ could be computed before iterations, since we have determined $\{\eta_i\}$ in advance, so it will not introduce extra computational cost. The most demanding part of conjugate gradient method is calculating its left hand side $A(\eta_i)\mathbf{m}$, because it contains a Fourier transform of $P\mathbf{m}$ from time domain to frequency domain and an inverse Fourier transform of $N(\eta_i)^{-1}P\mathbf{m}$ from frequency domain back to time domain, which is order $\mathcal{O}(n \log n)$ with n being the length of time ordered data. Compare to traditional conjugate gradient method, we swap N^{-1} with $N(\eta)^{-1}$, and the cost is the same, since both methods need a fast Fourier transform and inverse fast Fourier transform at one iteration. Therefore the computational cost it the same for one step.

In Appendix A our analysis is based on $\chi^2(\hat{\mathbf{m}}(\eta_i), \eta_i)$ which is evaluated at $\hat{\mathbf{m}}(\eta_i)$ the estimated map at η_i . So we should update η_i to η_{i+1} when the map from our calculation $\mathbf{m} \approx \hat{\mathbf{m}}(\eta_i)$. How do we know this condition is satisfied? Since for each new η_i value, we are solving a new set of linear equations (5), and we could stop calculation and moving to next value η_{i+1} when the norm of residual $\|\mathbf{r}(\mathbf{m}, \eta_i)\|$ is small, see Eq. (7). Calculation of the residual vector $\mathbf{r}(\mathbf{m}, \eta_i)$ is part of conjugate gradient algorithm, so this will not add extra cost either. Therefore, overall introducing η will not have extra computational cost.

However, we start a new conjugate gradient algorithm whenever η_i updates to η_{i+1} , which means the residual $\mathbf{r}(\mathbf{m}, \eta_{i+1})$ need to be calculated based on new η_{i+1} . Thus must re-initialize the conjugate gradient algorithm when η changes. This residual calculation contains an extra $A(\eta_i)\mathbf{m}$ operation. Therefore, if we have a series $\eta_1, \eta_2, \eta_3, \dots, \eta_{n_\eta}$, there will have $n_\eta - 1$ extra $A(\eta)\mathbf{m}$

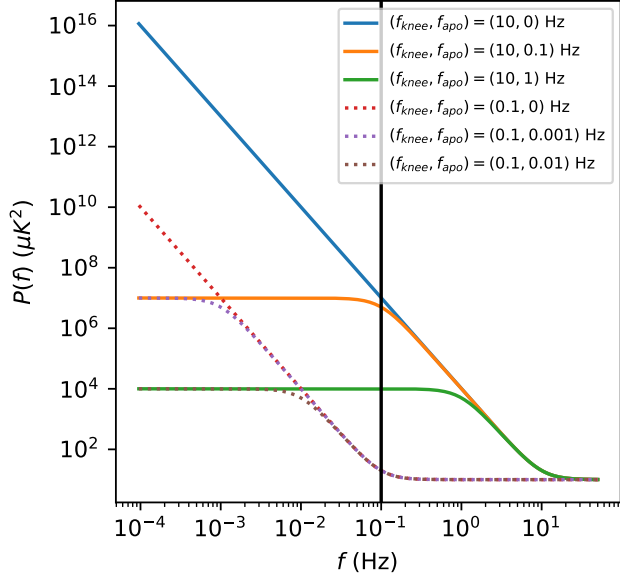


Figure 1. Noise power spectra that we use in our map-making simulations. These show a variety of low-frequency behavior, parameterized by Eq. (9), with white-noise level $\sigma^2 = 10 \mu\text{K}^2$ and low-frequency power-law slope $\alpha = 3$. Here we show two knee frequencies, $f_{\text{knee}} = 10$ Hz (solid lines) and $f_{\text{knee}} = 0.1$ Hz (dashed lines). For each knee frequency, we have shown an unflattened spectrum ($f_{\text{apo}} = 0$ Hz), and two flattened ones ($f_{\text{apo}} = 0.1f_{\text{knee}}$ and $0.01f_{\text{knee}}$). The vertical line shows our scanning frequency.

operations compare to traditional conjugate gradient method. If the total number of iterations is much larger than the number of η parameters n_η , then this extra cost is negligible. For our simulation, this extra step would have rather significant impact on final result. To have a fair comparison between parameterized and traditional conjugate gradient method, we will present our results with number of $P^\dagger N(\eta)^{-1} P \mathbf{m}$ operations as horizontal axis.

2.5. Numerical Simulations

To compare these algorithms, we need to do some simple simulation of scanning processes, and generate time ordered data from a random sky signal.¹ Our sky is a small rectangular area, with two orthogonal directions x and y , both with range from -1° to $+1^\circ$. The signal has stokes parameters (I, Q, U) for intensity and linear polarization.

For the scanning process, our mock telescope contains nine detectors, each with different sensitivity to polarization Q and U . It scans the sky with a raster scanning

¹ The source code and other information are available at https://github.com/Bai-Qiang/map_making_perturbative_approach

pattern and scanning frequency $f_{\text{scan}} = 0.1$ Hz and sampling frequency $f_{\text{sample}} = 100$ Hz. The telescope scans the sky horizontally and then vertically, and then digitizes the position (x, y) into 512×512 pixels. This gives noiseless signal $\mathbf{s} = P \mathbf{m}$.

We model the noise power spectrum with

$$P(f) = \sigma^2 \left(1 + \frac{f_{\text{knee}}^\alpha + f_{\text{apo}}^\alpha}{f^\alpha + f_{\text{apo}}^\alpha} \right) \quad (9)$$

which is white at high frequencies, a power law below the knee frequency, and gives us the option to flatten the low-frequency noise below an apodization frequency (like in Papež et al. 2018). Note that as $f_{\text{apo}} \rightarrow 0$, $P(f) \rightarrow \sigma^2(1 + (f/f_{\text{knee}})^{-\alpha})$, and it becomes a $1/f$ -type noise model.

Dünner et al. (2013) measured the slopes of the atmospheric noise in the Atacama under different water vapor conditions, finding $\alpha = 2.7$ to 2.9 . Here we use $\sigma^2 = 10 \mu\text{K}^2$, $\alpha = 3$, and compare the performance under different noise models. In our calculations we choose different combination of f_{knee} and f_{apo} . Some of the power spectrum are shown in Figure 1. The noise spectra with the most low frequency noise have high f_{knee} or low cut-off f_{apo} .

The noise covariance matrix

$$N_{ff'} = P(f) \frac{\delta_{ff'}}{\Delta_f} \quad (10)$$

is a diagonal matrix in frequency space, where Δ_f is equal to reciprocal of total scanning time $T \approx 1.05 \times 10^4$ seconds.

Finally, we get the simulated time ordered data $\mathbf{d} = \mathbf{s} + \mathbf{n}$ by adding up signal and noise.

3. RESULTS

We first compare the standard conjugate gradient method with simple preconditioner $P^\dagger P$ versus conjugate gradient with our perturbed linear system. Figure 2 shows the $\chi^2(\mathbf{m})$ results for a $1/f$ noise model ($f_{\text{apo}} = 0$) with different knee frequencies. Note that the χ^2 values in all figures are calculated based on the standard $\chi^2(\mathbf{m})$ in Eq. (3), not the $\chi^2(\mathbf{m}, \eta)$ of the modified system (Eq. A1). The target minimum χ_{min}^2 is calculated from a deliberately slowed and well-converged parameterized conjugate gradient method, one with 100 η values and that halts when the final norm of the residual $\|\mathbf{r}(\mathbf{m}, 1)\|$ is smaller than $10^{-5} \times \|P^\dagger N^{-1} \mathbf{d}\|$, or 100 iterations after $\eta = 1$. From Figure 2 we can see for the $1/f$ noise model, when $f_{\text{knee}} \gtrsim 10f_{\text{scan}}$ the parameterized method starts showing advantage over vanilla conjugate gradient method.

In Figure 3, we fixed $f_{\text{knee}} = 10$ Hz, and change f_{apo} . When f_{apo} is much smaller than f_{knee} the parameterized

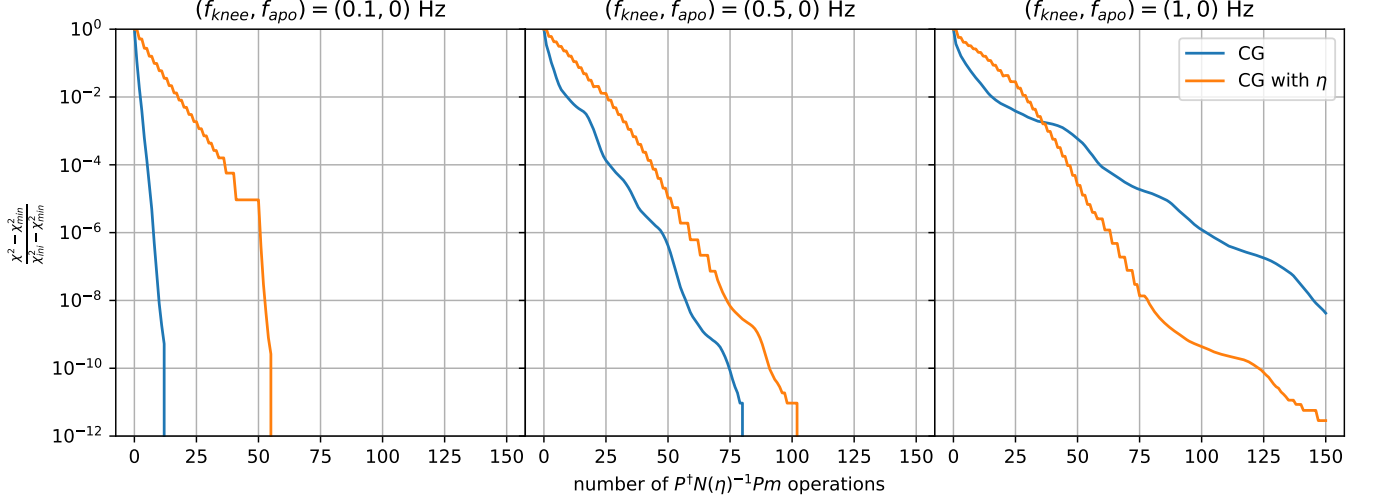


Figure 2. Convergence properties depend on the amount of low-frequency noise, which increases with increasing knee frequency from the left panel to the right. Here we show the $\chi^2(\mathbf{m})$ with respect to number of iterations. The map-making equation (2) minimize the $\chi^2(\mathbf{m})$, so the curve which falls fastest is the preferred method. We compare the traditional conjugate gradient method (“CG,” blue line) with the parameterized conjugate gradient method (“CG with η ,” orange line) under different $1/f$ noise models (fixed $f_{\text{apo}} = 0$ Hz but different f_{knee} in Eq.(9)). When $f_{\text{knee}} \gtrsim 10 f_{\text{scan}} = 1$ Hz, there are significant amount of low-frequency noise and the parameterized conjugate gradient method starts showing advantages. The vertical axis is rescaled such that all curves start from 1.

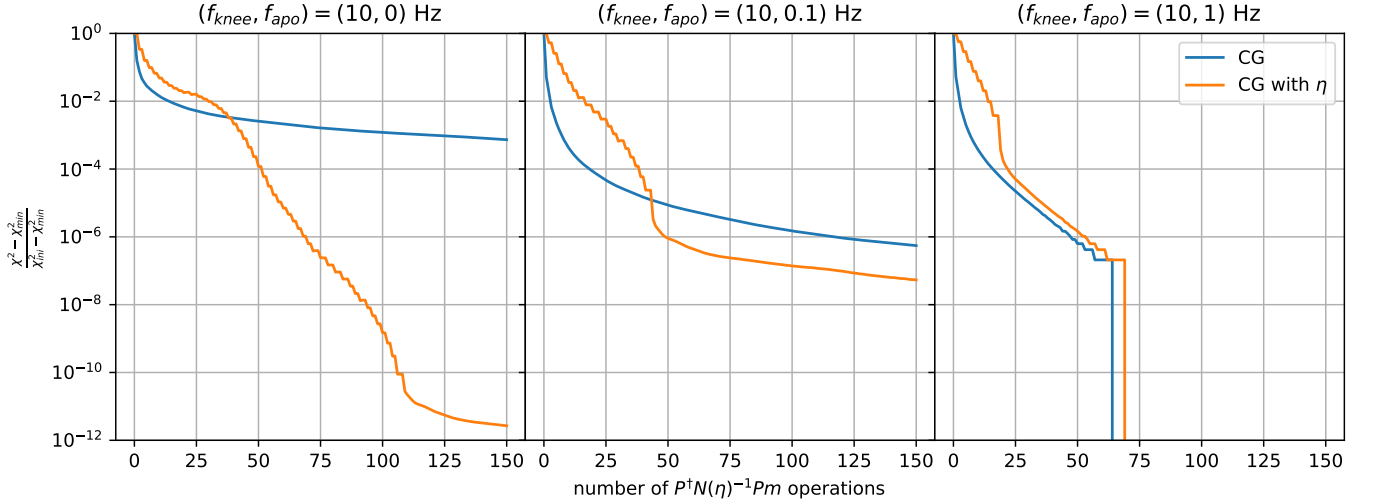


Figure 3. Like Figure 2, but adjusting the low-frequency noise by flattening it with an apodization parameter. Low-frequency noise decreases with increasing apodization frequency from left to right. We compare the traditional conjugate gradient method (“CG,” blue line) with the parameterized conjugate gradient method (“CG with η ,” orange line). When f_{apo} is much smaller than f_{knee} , there a lot of low-frequency noise and the parameterized conjugate gradient method is better (falls faster) than the traditional one.

conjugate gradient method performs better. As we increase f_{apo} while fix f_{knee} , eventually these two methods perform similarly.

If we look at the power spectrum in Figure 1, when f_{knee} is small or f_{apo} is large there is not much low-frequency noise. So we conclude that the introduction of the slowly-varying η parameter could improve perfor-

mance most when there are large low-frequency noise contributions.

We also tried different $1/f$ noise slopes α . For $\alpha = 2$, the conclusion is the same as $\alpha = 3$. When $\alpha = 1$, the low-frequency noise is reduced compared to the cases with steeper slopes, and the vanilla conjugate gradient method is preferred, except some cases with very large knee frequency like $f_{\text{knee}} = 100$ Hz and $f_{\text{apo}} = 0$

which favors the parameterized method. In Papež et al. (2018), the slope $\alpha = 1$ and the noise power spectrum is flattened at $f_{\text{apo}} \approx 0.1 f_{\text{knee}}$. Their knee frequency is the same as scanning frequency, so is most like our case when $f_{\text{knee}} = f_{\text{scan}} = 0.1$ Hz. Their case had little low-frequency noise, and we confirm their result that the standard conjugate gradient method converges faster in that case. In general, however, we find cases with significantly more low-frequency noise benefit from the cooling/parameterized approach.

4. CONCLUSIONS

We analyzed a parameterized conjugate gradient mapmaking method inspired by the messenger-field idea of separating the white noise out of noise covariance matrix. Then we gave an analytical expression for the series of η parameters, and showed that this method would not introduce extra computational cost compared to a traditional conjugate method.

We tested this method under different power spectrum, both flattened and non-flattened at low frequency. The results showed that the parameterized method is faster than the traditional conjugate gradient method when there is a significant amount of low-frequency noise. It could be further improved if we could get a more accurate estimation for the change in χ^2 as a function of the η parameter, either before iteration or without using time ordered data during iteration.

APPENDIX

A. THE DERIVATION OF η SERIES

We know that initial degree of heteroscedasticity $\eta_0 = 0$, which means the system is homoscedastic (uniform noise) to start. What would be a good value for the next parameter η_1 ? To simplify notation, we use N_η to denote the parameterized covariance matrix $N(\eta) = \tau I + \eta \bar{N}$. For some specific η value, the estimated map $\hat{\mathbf{m}}(\eta) = (P^\dagger N_\eta^{-1} P)^{-1} P^\dagger N_\eta^{-1} \mathbf{d}$ minimizes

$$\chi^2(\mathbf{m}, \eta) = (\mathbf{d} - P\mathbf{m})^\dagger N_\eta^{-1} (\mathbf{d} - P\mathbf{m}). \quad (\text{A1})$$

with η being fixed. We restrict to the case that the noise covariance matrix N is diagonal in the frequency domain, and represent the frequency-domain eigenvalues as N_f .

The perturbative scheme works like this. We start with $\chi^2(\hat{\mathbf{m}}(\eta_0), \eta_0)$ with $\hat{\mathbf{m}}(\eta_0) = (P^\dagger P)^{-1} P^\dagger \mathbf{d}$ which could be solved directly. Then we use conjugate gradient method to find $\hat{\mathbf{m}}(\eta_1)$ and the corresponding χ^2 value is $\chi^2(\hat{\mathbf{m}}(\eta_1), \eta_1)$. So let us consider $\eta_1 = \eta_0 + \delta\eta = \delta\eta$ such that $\eta_1 = \delta\eta$ is very small quantity, $\delta\eta \ll 1$. (Remember $\eta_0 = 0$.) Since $\hat{\mathbf{m}}(\eta)$ minimizes $\chi^2(\mathbf{m}, \eta)$ with η being fixed, we have $\frac{\partial}{\partial \mathbf{m}} \chi^2(\hat{\mathbf{m}}(\eta), \eta) = 0$, and using the chain rule

$$\frac{d}{d\eta} \chi^2(\hat{\mathbf{m}}(\eta), \eta) = \frac{\partial}{\partial \eta} \chi^2(\hat{\mathbf{m}}(\eta), \eta) = -(\mathbf{d} - P\hat{\mathbf{m}}(\eta))^\dagger N_\eta^{-1} \bar{N} N_\eta^{-1} (\mathbf{d} - P\hat{\mathbf{m}}(\eta)) \quad (\text{A2})$$

Also note that we fixed the preconditioner as $M = P^\dagger P$ during our calculation, this parameterizing process could be applied to any preconditioner and possibly improve performance when there is significant amount of low-frequency noise.

This type of estimate for the cooling parameter may also be apply to other areas, like the Wiener filter. Papež et al. (2018) showed that the messenger field method of Elsner & Wandelt (2013) for solving Wiener filter problem could also be written as parameterized conjugate gradient algorithm. That system also may benefit from an analysis of the signal-to-noise properties and when splitting and parameterizing the noise covariance improves performance. (Kodi Ramanah et al. (2017) also suggests to split the signal covariance for the Wiener filter and combine the uniform parts of the signal and noise.)

The benefits to mapmaking from a cooled messenger method seem to come from the cooling and not actually from the messenger field that inspired it. However, the messenger field approach may still have a role in the analysis of CMB maps. In particular, the close connection between the messenger method and Gibbs sampling may allow us to cheaply generate noise realizations of a converged map by generating samples from the map posterior distribution, something that we will continue to explore in future work.

BQ and KH are supported by NSF award 1815887.

Then the fractional decrease of $\chi^2(\hat{\mathbf{m}}(\eta_0), \eta_0)$ from η_0 to $\eta_1 = \delta\eta$ is

$$-\frac{\delta\chi^2(\hat{\mathbf{m}}(\eta_0), \eta_0)}{\chi^2(\hat{\mathbf{m}}(\eta_0), \eta_0)} = -\delta\eta \frac{\frac{d}{d\eta}\chi^2(\hat{\mathbf{m}}(\eta_0), \eta_0)}{\chi^2(\hat{\mathbf{m}}(\eta_0), \eta_0)} = \delta\eta \frac{1}{\tau} \frac{(\mathbf{d} - P\hat{\mathbf{m}}(\eta_0))^\dagger \bar{N}(\mathbf{d} - P\hat{\mathbf{m}}(\eta_0))}{(\mathbf{d} - P\hat{\mathbf{m}}(\eta_0))^\dagger (\mathbf{d} - P\hat{\mathbf{m}}(\eta_0))} \quad (\text{A3})$$

Here we put a minus sign in front of this expression such that it's non-negative, and use $N_{\eta=0} = \tau I$ at the second equality. We want $|\delta\chi^2(\hat{\mathbf{m}}(\eta_0), \eta_0)| = \chi^2(\hat{\mathbf{m}}(\eta_0), \eta_0) - \chi^2(\hat{\mathbf{m}}(\eta_1), \eta_1)$ to be large such that it could converge fast. Which means $\chi^2(\hat{\mathbf{m}}(\eta_1), \eta_1)$ is much smaller than $\chi^2(\hat{\mathbf{m}}(\eta_0), \eta_0)$, or $\chi^2(\hat{\mathbf{m}}(\eta_1), \eta_1) \ll \chi^2(\hat{\mathbf{m}}(\eta_0), \eta_0)$. Then we would expect

$$-\frac{\delta\chi^2(\hat{\mathbf{m}}(0), 0)}{\chi^2(\hat{\mathbf{m}}(0), 0)} = 1 - \frac{\chi^2(\hat{\mathbf{m}}(\eta_1), \eta_1)}{\chi^2(\hat{\mathbf{m}}(0), 0)} \approx 1^- \quad (\text{A4})$$

The upper bound is strictly smaller than 1. Now we could use Eq.(A3) and let it equal to 1, then $\delta\eta = -\chi^2(\hat{\mathbf{m}}(\eta_0), \eta_0) / \frac{d}{d\eta}\chi^2(\hat{\mathbf{m}}(\eta_0), \eta_0)$. However if we apply this idea to $\eta_{m+1} = \eta_m + \delta\eta_m$ with $m \geq 1$, we would get

$$\delta\eta_m = -\chi^2(\hat{\mathbf{m}}(\eta_m), \eta_m) / \frac{d}{d\eta}\chi^2(\hat{\mathbf{m}}(\eta_m), \eta_m). \quad (\text{A5})$$

As mentioned before, we need to determine the entire series $\{\eta_i\}$ before conjugate gradient iterations, and we could not calculate $\hat{\mathbf{m}}(\eta_m)$ directly because of the difficulty of matrix inversions. Therefore we could not get $\delta\eta_m$ values in advance. That means we need to find another approach.

Let us go back to Eq.(A3). Since it is hard to analyze $\mathbf{d} - P\hat{\mathbf{m}}(\eta)$ under frequency domain, we treat it as an arbitrary vector, then the least upper bound of Eq.(A3) is given by

$$-\frac{\delta\chi^2(\hat{\mathbf{m}}(\eta_0), \eta_0)}{\chi^2(\hat{\mathbf{m}}(\eta_0), \eta_0)} \leq \frac{\delta\eta}{\tau} \max(\bar{N}_f) \quad (\text{A6})$$

where $\max(\bar{N}_f)$ is the maximum eigenvalue of \bar{N} . We want $-\frac{\delta\chi^2(\hat{\mathbf{m}}(\eta_0), \eta_0)}{\chi^2(\hat{\mathbf{m}}(\eta_0), \eta_0)}$ to be as large as possible, but it won't exceed 1. If we combine Eq. (A4) and Eq. (A6), and choose $\delta\eta$ such that the least upper bound is equal to 1, to make sure the process would not go too fast. Thus we have

$$\eta_1 = \frac{\tau}{\max(\bar{N}_f)} = \frac{\min(N_f)}{\max(N_f) - \min(N_f)}. \quad (\text{A7})$$

Here N_f and \bar{N}_f are the eigenvalues of N and \bar{N} in the frequency domain. If the condition number of noise covariance matrix $\kappa(N) = \max(N_f) / \min(N_f) \gg 1$, then $\eta_1 \approx \kappa^{-1}(N)$.

What about the other parameters η_m with $m > 1$? We use a similar analysis, letting $\eta_{m+1} = \eta_m + \delta\eta_m$ with a small $\delta\eta_m \ll 1$. First, let us find the least upper bound

$$-\frac{\delta\chi^2(\hat{\mathbf{m}}(\eta_m), \eta_m)}{\chi^2(\hat{\mathbf{m}}(\eta_m), \eta_m)} = \delta\eta_m \frac{(\mathbf{d} - P\hat{\mathbf{m}}(\eta_m))^\dagger N_{\eta_m}^{-1} \bar{N} N_{\eta_m}^{-1} (\mathbf{d} - P\hat{\mathbf{m}}(\eta_m))}{(\mathbf{d} - P\hat{\mathbf{m}}(\eta_m))^\dagger N_{\eta_m}^{-1} (\mathbf{d} - P\hat{\mathbf{m}}(\eta_m))} \quad (\text{A8})$$

$$\leq \delta\eta_m \max\left(\frac{\bar{N}_f}{\tau + \eta_m \bar{N}_f}\right) \quad (\text{A9})$$

The upper bound in the second line is a little bit tricky. Both matrix \bar{N} and $N_{\eta_m}^{-1}$ can be simultaneously diagonalized in frequency space. For each eigenvector \mathbf{e}_f , the corresponding eigenvalue of the matrix on the numerator $N_{\eta_m}^{-1} \bar{N} N_{\eta_m}^{-1}$ is $\lambda_f = \bar{N}_f (\tau + \eta_m \bar{N}_f)^{-2}$, and the eigenvalue for matrix on the denominator $N_{\eta_m}^{-1}$ is $\gamma_f = (\tau + \eta_m \bar{N}_f)^{-1}$. Their eigenvalues are related by $\lambda_f = [\bar{N}_f / (\tau + \eta_m \bar{N}_f)] \gamma_f$. For any vector $\mathbf{v} = \sum_f \alpha_f \mathbf{e}_f$, we have

$$\frac{\mathbf{v}^\dagger N_{\eta_m}^{-1} \bar{N} N_{\eta_m}^{-1} \mathbf{v}}{\mathbf{v}^\dagger N_{\eta_m}^{-1} \mathbf{v}} = \frac{\sum_f \alpha_f^2 \lambda_f}{\sum_f \alpha_f^2 \gamma_f} = \frac{\sum_f \alpha_f^2 \gamma_f \bar{N}_f / (\tau + \eta_m \bar{N}_f)}{\sum_f \alpha_f^2 \gamma_f} \leq \max\left(\frac{\bar{N}_f}{\tau + \eta_m \bar{N}_f}\right). \quad (\text{A10})$$

Again assuming $\chi^2(\hat{\mathbf{m}}(\eta_{m+1}), \eta_{m+1}) \ll \chi^2(\hat{\mathbf{m}}(\eta_m), \eta_m)$, which we expect it to be satisfied for $\eta_m \ll 1$. That is because if $\eta \lesssim 1$, $\chi^2(\hat{\mathbf{m}}(\eta), \eta)$ would close to the minimum χ^2 which means $\chi^2(\hat{\mathbf{m}}(\eta_{m+1}), \eta_{m+1}) \lesssim \chi^2(\hat{\mathbf{m}}(\eta_m), \eta_m)$,

which would violate our assumption. Luckily, the final result (A14) is a geometric series, only the last few η_m values fail to satisfy this condition. Similarly, we could set the least upper bound equal to 1. Then we get

$$\delta\eta_m = \min\left(\frac{\tau + \eta_m \bar{N}_f}{\bar{N}_f}\right) = \eta_m + \frac{\tau}{\max(\bar{N}_f)}. \quad (\text{A11})$$

Therefore

$$\eta_{m+1} = \eta_m + \delta\eta_m = 2\eta_m + \frac{\tau}{\max(\bar{N}_f)} \quad (\text{A12})$$

The final term $\tau/\max(\bar{N}_f) = \eta_1$ becomes subdominant after a few terms, and we see that the η_m increase like a geometric series. If written in the form $\eta_{m+1} + \tau/\max(\bar{N}_f) = 2(\eta_m + \tau/\max(\bar{N}_f))$ it's easy to see that for $m \geq 1$, $\eta_m + \tau/\max(\bar{N}_f)$ forms a geometric series

$$\eta_m + \frac{\tau}{\max(\bar{N}_f)} = \left(\eta_1 + \frac{\tau}{\max(\bar{N}_f)}\right) 2^{m-1} = \frac{\tau}{\max(\bar{N}_f)} 2^m \quad (\text{A13})$$

where we used $\eta_1 = \tau/\max(\bar{N}_f)$. Note that $m = 0$ and $\eta_0 = 0$ also satisfy this expression and we've got final expression for all η_m

$$\eta_m = \min\left\{1, \frac{\tau}{\max(\bar{N}_f)}(2^m - 1)\right\} \quad (\text{A14})$$

Here we need to truncate the series when $\eta_m > 1$.

We did some numerical simulation, and find that if we update η parameter based on Eq. A5, there is only marginally improvements over the η series given in Eq. A14 for the $1/f$ noise model, and slightly improvements when there is not many low frequency noise. If we use Eq. A5, it ends up with some less η parameters, but the interval between η_i and η_{i+1} gets larger. In our simulation this sometimes causes one more iteration at certain η value, so at the end there is only slightly improvements. For large data set that need lots of iteration to converge from η_i to η_{i+1} , where several extra calculation may not be significant, using Eq. A5 may have larger performance boost.

REFERENCES

- | | |
|----------------------------------------------------------------------------------------------------------------------------------------------------------------------------------------------------------------------------------------------------------------------------------------------------------------------------------------------------------------------------------------------------------------------------------------------------------------------------------------------------------------------------------------------------------------|------------------------------------------------------------------------------------------------------------------------------------------------------------------------------------------------------------------------------------------------------------------------------------------------------------------------------------------------------------------------------------------------------------------------------------------------------------------------------------------------------------------------------------------------------------------------------------------------------------------------------------------------------------|
| <p>487 Dünner, R., Hasselfield, M., Marriage, T. A., et al. 2013,
 488 ApJ, 762, 10, doi: 10.1088/0004-637X/762/1/10
 489 Elsner, F., & Wandelt, B. D. 2013, A&A, 549, A111,
 490 doi: 10.1051/0004-6361/201220586
 491 Huffenberger, K. M., & Næss, S. K. 2018, The
 492 Astrophysical Journal, 852, 92,
 493 doi: 10.3847/1538-4357/aa9c7d</p> | <p>494 Janssen, M. A., & Gulkis, S. 1992, in NATO Advanced
 495 Science Institutes (ASI) Series C, ed. M. Signore &
 496 C. Dupraz, Vol. 359 (Springer), 391–408
 497 Kodi Ramanah, D., Lavaux, G., & Wandelt, B. D. 2017,
 498 MNRAS, 468, 1782, doi: 10.1093/mnras/stx527
 499 Papež, J., Grigori, L., & Stompör, R. 2018, A&A, 620, A59,
 500 doi: 10.1051/0004-6361/201832987
 501 Tegmark, M. 1997, ApJL, 480, L87, doi: 10.1086/310631</p> |
|----------------------------------------------------------------------------------------------------------------------------------------------------------------------------------------------------------------------------------------------------------------------------------------------------------------------------------------------------------------------------------------------------------------------------------------------------------------------------------------------------------------------------------------------------------------|------------------------------------------------------------------------------------------------------------------------------------------------------------------------------------------------------------------------------------------------------------------------------------------------------------------------------------------------------------------------------------------------------------------------------------------------------------------------------------------------------------------------------------------------------------------------------------------------------------------------------------------------------------|